4 December 1998

ELSEVIER

Chemical Physics Letters 297 (1998) 491–498

CHEMICAL PHYSICS LETTERS

Dispersion studies of non-linear absorption in C_{60} using *Z*-scan

S. Venugopal Rao [a], D. Narayana Rao [a,*], J.A. Akkara [b], B.S. DeCristofano [b], D.V.G.L.N. Rao [c]

[a] *School of Physics, University of Hyderabad, Hyderabad-500 046, India*
[b] *US Army Natick R D&E Center, Natick, MA 01760, USA*
[c] *Department of Physics, University of Massachusetts, Boston, MA 02125, USA*

Received 24 August 1998; in final form 28 September 1998

Abstract

We present our experimental and theoretical results on the dispersion studies of non-linear absorption in C_{60} solution. Open-aperture *Z*-scans are performed over the visible region (440–660 nm) using an ns OPO. Our results are interpreted using a 5-level model taking into account both the excited state absorption and two-photon absorption processes. Results indicate that the excited state absorption dominates in the shorter-wavelength region (440–560 nm) whereas the two-photon absorption dominates in the longer-wavelength region (580–660 nm). © 1998 Elsevier Science B.V. All rights reserved.

1. Introduction

Optical limiters are devices that strongly attenuate optical beams at high intensities while exhibiting higher transmittance at low intensities. Such devices are useful for the protection of the human eye and optical sensors from intense laser beams. The development of materials for optical limiting is based on various mechanisms [1] such as free-carrier absorption and refraction in semiconductors, optical breakdown-induced scattering, thermal refractive beam spreading, two-photon absorption (TPA) and excited state absorption (ESA). Studies have shown very high performance ESA or reverse saturable absorption (RSA) behaviour in C_{60} [2–14]. These materials are characterised by their strong excited state absorption compared to ground state absorption. Most of these materials were studied either at 532 or 600 nm and the models used to evaluate the photo-physical parameters were based on either 4-level (first excited singlet and triplet levels) or 3-level (singlet levels only) models. For fs and ps pulse excitation, the triplet level contribution to the non-linear absorption can be neglected due to the slower intersystem crossing. Whereas with ns pulses the triplet levels do play an important role. Depending on the pump intensity and wavelength, the absorption could be: (1) from ground state S_0 to the first excited singlet state S_1 and then to the T_1 state through intersystem crossing, (2) directly from the S_0 to S_n states (TPA), (3) from the first excited singlet state S_1 to higher excited states S_n (ESA/RSA), or (4) from the T_1 to T_n states (ESA/RSA). One has to incorporate all these absorption phenomena in rate equations in order to obtain the exact contribution from each of these processes. Earlier reports [15–17] on dispersion studies of non-linear absorption do not take into consideration the contribution of two-photon absorption. We have performed an open-aperture *Z*-scan of C_{60}

* Corresponding author. E-mail: dnrsp@uohyd.ernet.in

0009-2614/98/$ - see front matter
PII: S0009-2614(98)01166-X

(in toluene) in the visible region from 440 to 660 nm. To fit our experimental data, we consider a theoretical model where a contribution to the nonlinear absorption could be from S_0 to S_n states (due to direct TPA), S_1 to S_n states (due to ESA/RSA) or T_1 to T_n states (due to ESA/RSA). Different curves are obtained theoretically by varying the ESA and TPA coefficients and the input intensity. The behaviour of the open-aperture *Z*-scan curve with changes in the above parameters is discussed in detail.

2. Experiment

Fig. 1a depicts the experimental arrangement and Fig. 1b details the 5-level model. We employ a commercial optical parametric oscillator (OPO) (MOPO laser by Spectra Physics) pumped by the third harmonic (355 nm) from the Quanta Ray Nd:YAG laser with a repetition rate of 10 Hz and tunable in the range of 380–1000 nm for the open-aperture *Z*-scan [18] studies. The experimental arrangement consists of a lens, sample and a large-area detector. The sample cell is moved along a rail to vary the intensity of light in the sample. The pulse duration of the laser is 6 ns. An aperture of 1.4 mm is used at the output of the MOPO laser to obtain a smooth profile in the far field. Energy after the aperture varied from 0.2 to 2 mJ/pulse, depending on the wavelength. The focal length of the lens used for focusing the beam into the sample is 50 mm. 1 mm glass cuvettes were used for the sample solutions. The input energy is monitored using a fast photo-diode and the output is measured using a similar photo-diode. C_{60} (> 99% pure) was bought from Strem Chemicals (USA) and dissolved in toluene to make $\sim 10^{-4}$–10^{-3} M solutions. The absorption spectrum of the C_{60} sample matches that reported in the literature. Open-aperture *Z*-scans are obtained in the wavelength region from 440 to 680 nm. The values of the beam waist at focus are $\sim$ 30–50 μm and the corresponding peak intensities are $\sim 10^8$–10^9 W/cm^2. The Rayleigh ranges are $\sim$ 6.5–8 mm depending on the wavelength and the input energy. Rate equations for the 5-level model shown in Fig. 1b are:

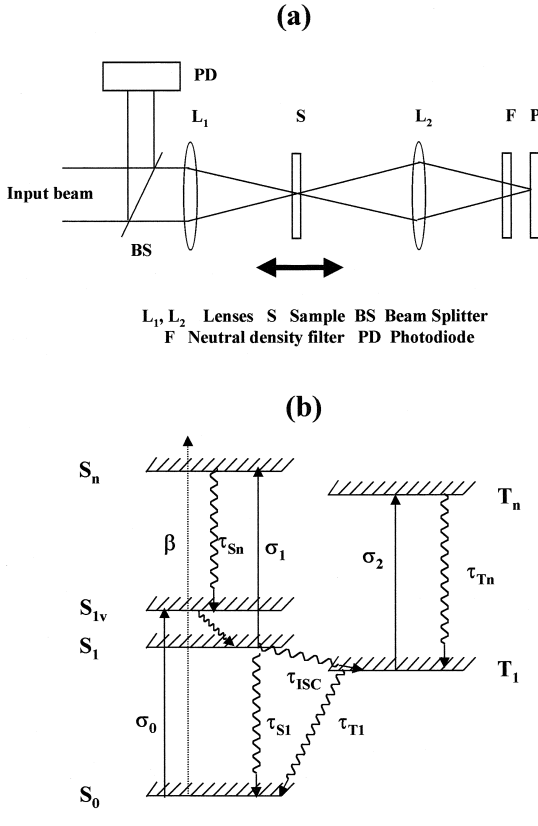

Fig. 1. (a) Experimental arrangement used for an open-aperture *Z*-scan. (b) Energy level diagram of a typical dye molecule. Radiative transitions are indicated by straight lines and non-radiative transitions by wavy lines.

$$\frac{dN_0}{dt} = -\frac{\sigma_0 I N_0}{\hbar\omega} - \frac{\beta I^2}{2\hbar\omega} + \frac{N_1}{\tau_1} + \frac{N_3}{\tau_4}, \tag{1}$$

$$\frac{dN_1}{dt} = -\frac{\sigma_1 I N_1}{\hbar\omega} + \frac{\sigma_0 I N_0}{\hbar\omega} - \frac{N_1}{\tau_1} - \frac{N_1}{\tau_{ISC}} + \frac{N_2}{\tau_2}, \tag{2}$$

$$\frac{dN_2}{dt} = \frac{\sigma_1 I N_1}{\hbar\omega} + \frac{\beta I^2}{2\hbar\omega} - \frac{N_2}{\tau_2}, \tag{3}$$

$$\frac{dN_3}{dt} = -\frac{\sigma_2 I N_3}{\hbar\omega} - \frac{N_3}{\tau_4} + \frac{N_1}{\tau_{ISC}} + \frac{N_4}{\tau_3}, \tag{4}$$

$$\frac{dN_4}{dt} = \frac{\sigma_2 I N_3}{\hbar\omega} - \frac{N_4}{\tau_3}, \tag{5}$$

and the intensity transmitted through the sample is given by

$$\frac{dI}{dz} = -\sigma_0 IN_0 - \sigma_1 IN_1 - \sigma_2 IN_3 - \beta I^2, \quad (6)$$

with

$$I = I_{00}\left(\frac{\omega_0^2}{\omega^2(z)}\right)\exp\left(-\frac{t^2}{\tau_p^2}\right)\exp\left(-\frac{2r^2}{\omega^2(z)}\right) \quad (7)$$

and

$$\omega(z) = \omega_0\left\{1+\left(\frac{z}{z_0}\right)^2\right\}^{1/2}; \quad z_0 = \frac{\pi\omega_0^2}{\lambda},$$

where σ_0 is the ground state absorption cross-section, σ_1 and σ_2 are the excited state absorption cross-sections from the S_1 and T_1 states, respectively; N_i's are the corresponding populations in the different states; τ_i's are the lifetimes of the excited states; z_0 is the Rayleigh range; ω_0 is the beam waist at focus; I is the intensity as a function of r, t, and z; I_{00} is the peak intensity at the focus of the gaussian beam; τ_p is the input pulse width used; β is the two-photon cross-section; and τ_{ISC} is the intersystem crossing rate. The differential equations are solved numerically using the Runge–Kutta fourth-order method. The differential equations are first de-coupled and then integrated over time, length, and along the radial direction. Assuming the input beam to be a gaussian, the limits of integration for r, t, and z are varied from 0 to ∞, $-\infty$ to ∞, and 0 to L (length of the sample), respectively. A typical number of slices used for r, t, and z are 60, 30, and 5, respectively. σ_1, σ_2, and β are then estimated through a least-squares fit of the experimental data.

3. Results and discussion

Fig. 2 shows the experimental data (scattered points) and the theoretical fits (solid lines) obtained using the 5-level model for wavelengths ranging from 440 to 640 nm. The ground state absorption cross-sections for different wavelengths were calculated using $\sigma_0 = \alpha/N$, where α is the linear absorption and N is the density of molecules per cm^3. Depending on the wavelength, I_{00} is taken as $\sim 10^8$–10^9 W/cm^2, $\omega_0 \approx 30$–50 μm, $z_0 \approx 6.5$–8 mm. The relaxation time of the first excited singlet state τ_{S_1}, intersystem crossing time τ_{ISC} and the lifetime of the first excited triplet state τ_{T_1} are taken as 70 ps, 650 ps, and 280 μs, respectively. The relaxation times of the S_n and T_n states are taken as ~ 100 fs. Excitation wavelengths are indicated for each Z-scan curve. In the wavelength region from 440 to 540 nm, the experimental data fit better with $\beta = 0$ and in the wavelength region 580 to 640 nm, β dominates with a smaller contribution from σ_2 or σ_1. The effect of σ_1 on the Z-scan curves is shown in Fig. 3 for two arbitrary wavelengths, one in the 440–540 nm range and the other in the 580–640 nm range. Fig. 3a shows the theoretical curves generated at 480 nm for $\sigma_0 = 3.0\times10^{-18}$ cm^2, $\sigma_1 = 15.0\times10^{-18}$ cm^2, $\sigma_2 = 12.0\times10^{-18}$ cm^2, $\beta = 0.0$ (solid line); $\sigma_0 = 3.0\times10^{-18}$ cm^2, $\sigma_1 = 0.0$, $\sigma_2 = 12.0\times10^{-18}$ cm^2, $\beta = 0.0$ (dotted line). Fig. 3b shows the theoretical curves generated at 600 nm for $\sigma_0 = 1.65\times10^{-18}$ cm^2, $\sigma_1 = 6.60\times10^{-18}$ cm^2, $\sigma_2 = 6.60\times10^{-18}$ cm^2, $\beta = 2.25\times10^{-8}$ cm/W (solid line); $\sigma_0 = 1.65\times10^{-18}$ cm^2, $\sigma_1 = 0.0$, $\sigma_2 = 6.60\times10^{-18}$ cm^2, $\beta = 2.25\times10^{-8}$ cm/W (dotted line). It can be seen that there is very little effect on the open-aperture Z-scan curves due to σ_1, which is mainly due to the fact that we have taken τ_{S_1} to be 70 ps. Lifetimes of the S_1 state have been reported to be ~ 100 ps and ~ 1.2 ns by several groups [19–23]. Our studies performed through incoherent laser spectroscopy [24] have shown a lifetime for the S_1 state of 70 ps. We could obtain a reasonably good fit for σ_1 varying from 15×10^{-18} to 20×10^{-18} cm^2 with $\sigma_2 \approx 12\times10^{-18}$ cm^2. Therefore, there could be larger error in the values of σ_1 compared to σ_2. If fs pulses are used for excitation then we expect a contribution of σ_1 alone to the non-linear absorption, as the intersystem crossing would be too slow compared to the pulse duration. From the fs data, one can then exactly find out the contribution of σ_1. We are in the process of procuring the fs data in the wavelength region of 440–540 nm, where the ESA plays a dominant role compared to the TPA. The effect of varying τ_{S_1} on the Z-scan curves is shown in Fig. 4. Simulated curves for $\tau_{S_1} = 1.2$ ns and 70 ps are shown in Fig. 4a for 480 nm and in Fig. 4b for 600 nm. The dotted line is the curve with $\tau_{S_1} = 1.2$ ns and the solid line is the curve with $\tau_{S_1} = 70$ ps, with all other parameters remaining same. We clearly see

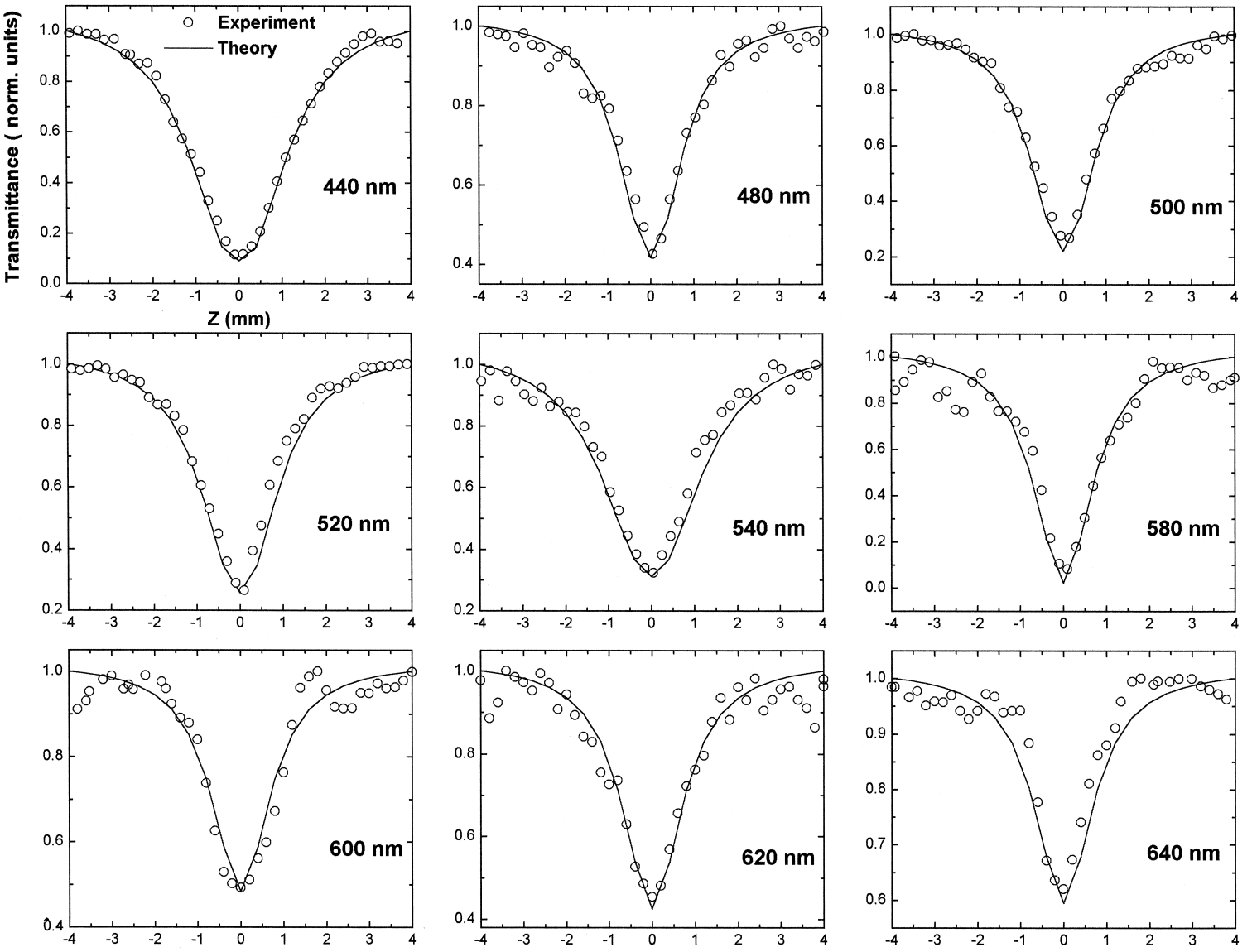

Fig. 2. Experimental data (open circles) and fitted curve (solid line) using the five-level model for different wavelengths (440–640 nm).

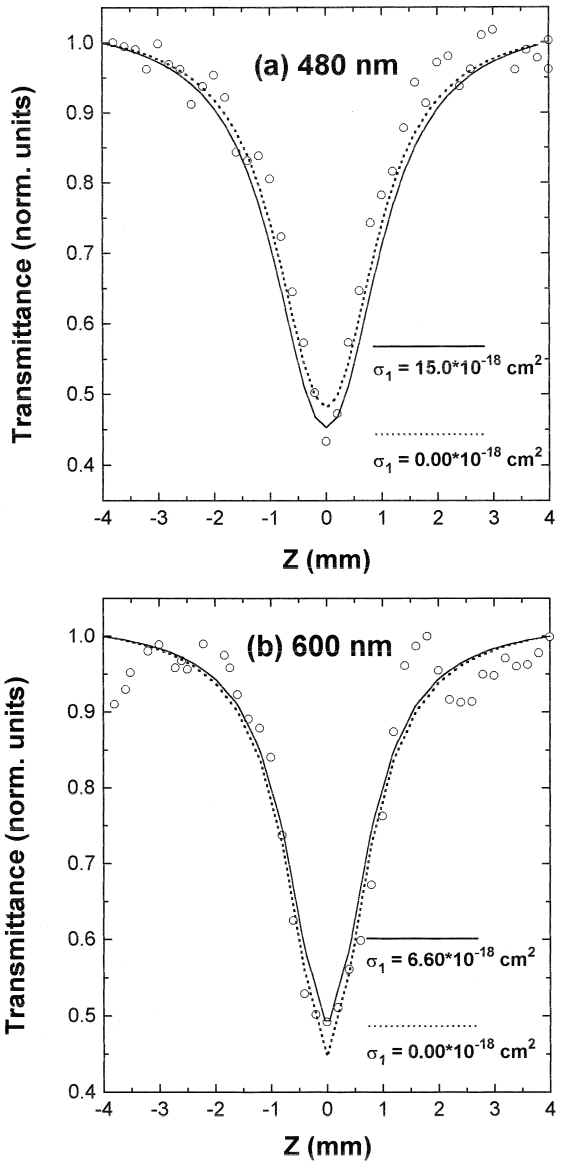

Fig. 3. Theoretical curves showing the effect of σ_1 at two wavelengths: (a) at 480 nm (and $\sigma_0 = 2.99\times10^{-18}$ cm^2, $\sigma_2 = 12.0\times10^{-18}$ cm^2, $\beta = 0.0$, $I_{00} = 10^9$ W/cm^2); and (b) at 600 nm (and $\sigma_0 = 1.65\times10^{-18}$ cm^2, $\sigma_2 = 2.4\times10^{-18}$ cm^2, $\beta = 2.25\times10^{-8}$ cm/W, $I_{00} = 4\times10^8$ W/cm^2). The scattered points are the experimental data, only for comparison.

that for $\tau_{S_1} = 1.2$ ns, the curves become very broad indicating that for the C_{60} sample, that was used in our system, $\tau_{S_1} = 70$ ps. For longer wavelengths (Fig. 4b), the effect of τ_{S_1} is small because of the domination of TPA in this range. The present results are therefore consistent with our earlier studies reported through degenerate 4-wave mixing (DFWM)

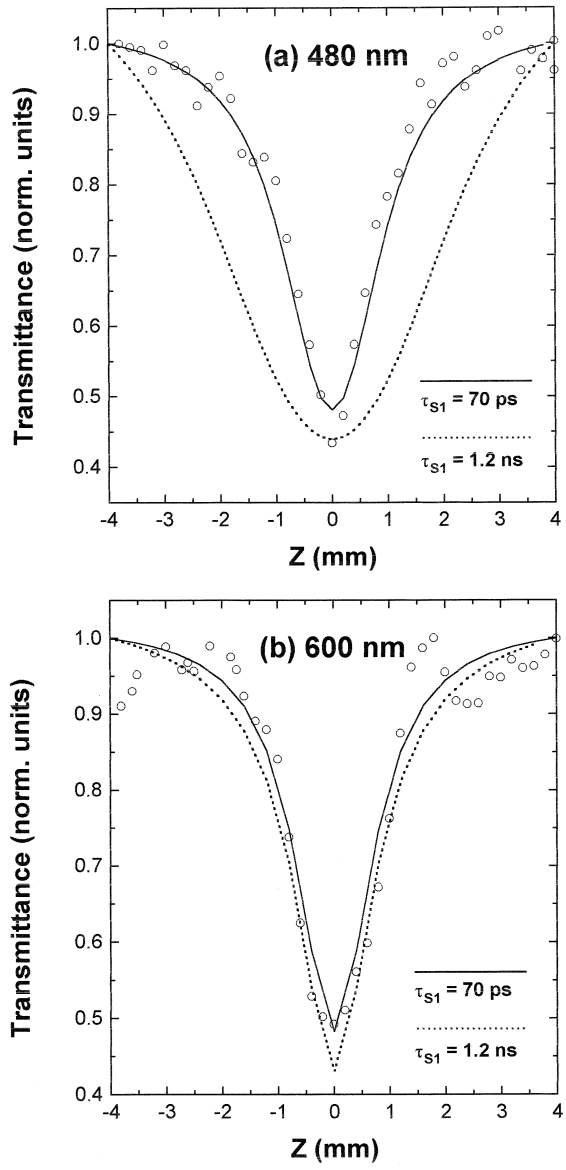

Fig. 4. Theoretical curves showing the effect of τ_{S_1} at two wavelengths: (a) at 480 nm (and $\sigma_0 = 2.99\times10^{-18}$ cm^2, $\sigma_1 = 0.0$, $\sigma_2 = 12.0\times10^{-18}$ cm^2, $\beta = 0.0$, $I_{00} = 10^9$ W/cm^2); and (b) at 600 nm (and $\sigma_0 = 1.65\times10^{-18}$ cm^2, $\sigma_1 = 6.6\times10^{-18}$ cm^2, $\sigma_2 = 2.4\times10^{-18}$ cm^2, $\beta = 2.25\times10^{-8}$ cm/W, $I_{00} = 4\times10^8$ W/cm^2). The scattered points are the experimental data, only for comparison.

experiments done with a broad band laser [24]. The sample that was used in both experiments is from the same batch and company.

σ_1, σ_2, and β values obtained from our results are given in Table 1 along with those reported in literature. There is no contribution from TPA (β) to the non-linear absorption before 540 nm. From 580 to 640 nm, the non-linear absorption appears to be dominated by TPA. Fig. 5 shows the influence of σ_2 and β on the theoretical curves. Fig. 5a shows the theoretical curves with and without σ_2 for 600 nm. Though both the fits can be seen to be close to the experimental data (open circles), the curve generated with non-zero σ_2 and β has a lower chi-square value. The σ_1 value was taken as zero in this region as we see from Fig. 3b that the contribution of σ_1 on the curves is negligible. The S_n and S_1 energies of C_{60} fall in the region of $\sim$29000 and $\sim$16000 cm^{-1}, respectively [26]. Excitations longer than 580 nm fall either on the lower edge of the absorption curve or below it. Since at such excitations it is expected that the molecule remains localized, without diffusing into the higher levels [27], eventually decaying into the S_0 level through τ_{S_1} or crossover to T_1 through τ_{ISC}. Under such circumstances σ_1 and β would have the same effect. A complete

Table 1
Comparison of the values obtained using our five-level model and those reported in the literature

σ_0 (10^{-18} cm^2)	σ_1 (10^{-18} cm^2)	σ_2 (10^{-18} cm^2)	β (10^{-8} cm W^{-1})	Refs.
1.21	8.07	5.35	–	Kost et al. [2]: 532 nm, 8 ns
2.87	15.7	9.22	–	Li et al. [3]: 532 nm, 15 ns
3.2	16.0	14	–	Barosso et al. [15]: 534 nm, 6 ns
				our study:
1.79	22.0	14.0	–	440 nm
2.99	12.8	9.6	–	480 nm
2.69	14.8	11.6	–	500 nm
2.70	22.2	11.4	–	520 nm
2.69	18.2	11.4	–	540 nm
1.445	–	3.0	2.45	580 nm
1.65	–	2.4	2.25	600 nm
1.03	–	3.6	1.95	620 nm
0.724	–	2.2	1.85	640 nm
α [a]	–	σ [b]	β_{eff}	McBranch et al. [10]: 6 ns,
3.4 cm^{-1}		0.39	0.96	561 nm
3.4 cm^{-1}		0.72	1.85	575 nm
0.45 cm^{-1}		0.45	0.18	680 nm
–	–	σ_2/σ_0	β_{eff}	Couris et al. [17]: 15 ns,
		–	3.9	620 nm
		8.3	3.14	630 nm
		7.5	1.9	640 nm
5.0	–	–	$\leq 3 \pm 1.5$	Bezel et al. [25]: 300 fs, 612 nm

[a] α = linear absorbance.
[b] σ = effective excited state cross-section.

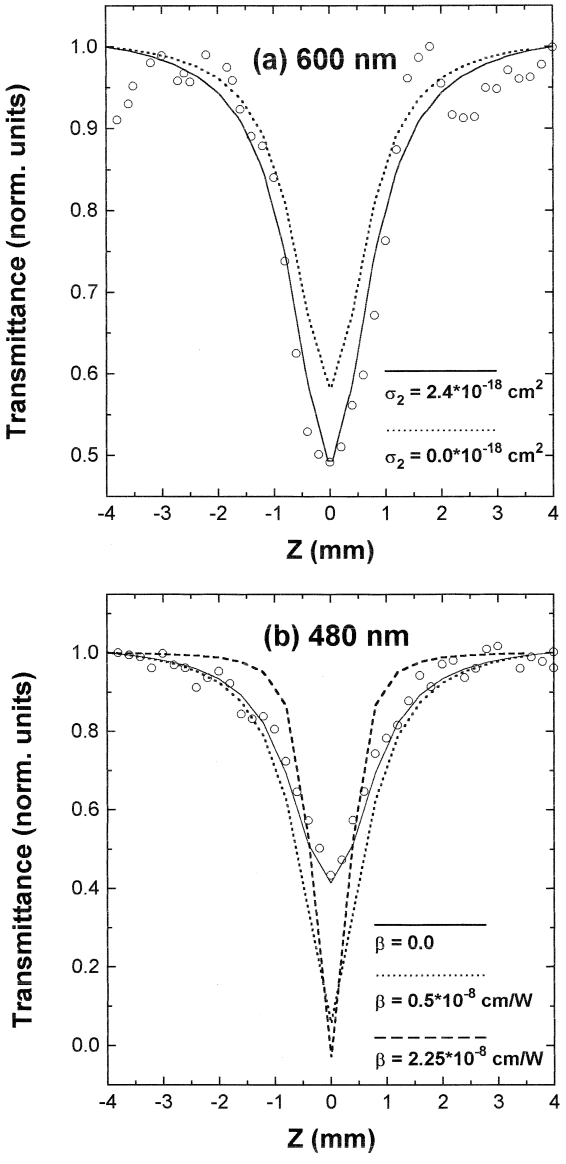

Fig. 5. Theoretical curves showing the effect of: (a) σ_2 at 600 nm with $\sigma_0 = 1.65\times10^{-18}$ cm^2, $\sigma_1 = 0.0$, $\beta = 2.25\times10^{-8}$ cm/W, $I_{00} = 4.6\times10^8$ W/cm^2; and (b) β at 480 nm with $\sigma_0 = 2.99\times10^{-18}$ cm^2, $\sigma_1 = 12.8\times10^{-18}$ cm^2, $\sigma_2 = 9.6\times10^{-18}$ cm^2, $I_{00} = 9.5\times10^8$ W/cm^2 and for dashed curve $\sigma_1 = 0.0$, $\sigma_2 = 0.0$, $I_{00} = 9.5\times10^8$ W/cm^2. The scattered points are the experimental data, only for comparison.

reversal in the domination of σ and β are observed in the region of short wavelengths. The introduction of a small value of β leads to a sharper valley, below 580 nm (Fig. 5b at 480 nm), deviating from the experimental values. The dotted curve is obtained with non-zero values of σ_1, σ_2 and $\beta = 0.5\times10^{-8}$ cm/W and the dashed curve is obtained for $\sigma_1 = \sigma_2 = 0.0$ and $\beta = 2.25\times10^{-8}$. This clearly shows the domination of σ_1 and σ_2 in the shorter-wavelength region

4. Conclusions

In conclusion, we have studied the dispersion behaviour of non-linear absorption in a C_{60} solution using open-aperture *Z*-scan. We have fitted our data using a 5-level model, taking into account both the non-linear absorption processes, ESA and TPA. We have derived information about the non-linear absorption processes from the shape of the open-aperture *Z*-scan curves. The main advantage of C_{60}, in comparison to porphyrins and phthalocyanines, is that it shows RSA behaviour over the entire visible region, either through ESA in the shorter wavelengths or through TPA in the longer-wavelength region.

Acknowledgements

DNR is a NRC fellow (USA). DNR thanks Professor S. Tripathy, University of Massachusetts, Lowell, for the experimental facilities and DST (India) for financial support. SVR thanks UGC for financial assistance.

References

[1] L.W. Tutt, T.F. Bogges, Prog. Quantum Elcetron. 17 (1993) 299.
[2] A. Kost, L.W. Tutt, M.B. Kelvin, T.K. Dougherty, W.E. Elias, Opt. Lett. 18 (1993) 334.
[3] C. Li, L. Zhang, R. Wang, Y. Song, Y. Wang, J. Opt. Soc. Am. B 11 (1994) 1356.
[4] V.V. Golovlev, W.R. Garrett, C.H. Chen, J. Opt. Soc. Am. B 13 (1996) 2801.
[5] Y. Sun, Q. Gong, S.C. Yang, Y.H. Zou, L. Fei, X. Zhou, D. Qiang, Opt. Commun. 102 (1993) 205.
[6] J.E. Wray, K.C. Liu, C.H. Chen, W.R. Garrett, M.G. Payne, R. Goedert, D. Templeton, Appl. Phys. Lett. 64 (1994) 2785.
[7] D. Vincent, J. Cruickshank, Appl. Opt. 36 (1997) 7794.
[8] M. Cha, N.S. Sariciftci, A.J. Heeger, J.C. Hummelen, F. Wudl, Appl. Phys. Lett. 67 (1995) 3580.

[9] K.M. Nashold, D.P. Walter, J. Opt. Soc. Am. B 12 (1995) 1228.
[10] D. McBranch, L. Smilowitz, V. Klimov, A. Koskelo, J.M. Robinson, B.R. Mattes, J.C. Hummelen, F. Wudl, J.C. Withers, N.F. Borrelli, Proc. SPIE (Soc. Photo-Opt. Instrum. Eng.) 2530 (1995) 196.
[11] R. Signorini, M. Zerbetto, M. Meneghetti, R. Bozio, M. Maggini, C.D. Faveri, M. Prato, G. Scorrano, Chem. Commun. (1996) 1891.
[12] J. Schell, D. Brinkmann, D. Ohlmann, B. Honerlage, R. Levy, M. Joucla, J.L. Rehspringer, J. Serughetti, C. Bovier, J. Chem. Phys. 108 (1998) 8599.
[13] K.M. Nashold, D.P. Walter, J. Opt. Soc. Am. B 12 (1995) 1228.
[14] S.R. Mishra, H.S. Rawat, M.P. Joshi, S.C. Mehendale, J. Phys. B: At. Mol. Phys. 27 (1994) L157.
[15] J. Barroso, A. Costela, I.G. Moreno, J.L. Saiz, J. Phys. Chem. A 102 (1998) 2527.
[16] F. Henari, J. Callaghan, H. Stiel, W. Blau, D.J. Cardin, Chem. Phys. Lett. 199 (1992) 144.
[17] S. Couris, E. Koudoumas, A.A. Ruth, S. Leach, J. Phys. B: At. Mol. Phys. 28 (1995) 4537.
[18] M. Sheik-Bahae, A.A. Said, T.H. Wei, D.J. Hagan, E.W. Stryland, IEEE J. Quantum Electron. 26 (1990) 760.
[19] R.A. Cheville, N.J. Halas, Phys. Rev. B 45 (1992) 4548.
[20] V.M. Farztdinov, Y.E. Lozovik, Y.A. Matveets, A.G. Stepanov, V.S. Letokhov, J. Phys. Chem. 98 (1994) 3290.
[21] I.E. Kardash, V.S. Letokhov, Y.E. Lozovik, Y.A. Matveets, A.G. Stepanov, V.M. Farztdinov, JETP Lett. 58 (1993) 138.
[22] T.W. Ebbesen, K. Tanigaki, S. Kuroshima, Chem. Phys. Lett. 181 (1991) 501.
[23] R.J. Sension, C.M. Phillips, A.Z. Szarka, W.J. Romanow, A.R. McGhie, J.P. McCauley Jr., A.B. Smith III, M. Hochstrasser, J. Phys. Chem. 95 (1991) 6075.
[24] S. Venugopal Rao, D. Narayana Rao, Chem. Phys. Lett. 283 (1998) 227.
[25] I.V. Bezel, S.V. Chekalin, Y.A. Matveets, A.G. Stepanov, A.P. Yartsev, V.S. Letokhov, Chem. Phys. Lett. 218 (1994) 475.
[26] M. Lee, O.K. Song, J.C. Seo, D. Kim, Y.D. Suh, S.M. Jin, S.K. Kim, Chem. Phys. Lett. 196 (1992) 325.
[27] G.B. Talapatra, D.N. Rao, P.N. Prasad, J. Phys. Chem. 88 (1984) 4636.